



ISSN: 0067-2904

## Effect of Fe<sub>2</sub>O<sub>3</sub> Nanoparticles Dust on the D.C Plasma Characteristics with Mirror Magnetron

Shahad Emaduldeen Abdulghani\*, Qusay A. Abbas

Department of Physics, College of Science, University of Baghdad, Baghdad, Iraq

Received: 11/6/2022

Accepted: 1/2/2023

Published: 30/5/2023

### Abstract

In this paper, the effect of iron oxide nanoparticles dust (Fe<sub>2</sub>O<sub>3</sub> NPs) on the parameters of DC electric discharge plasma under vacuum in argon gas was studied with the presence of a mirror magnetron behind the electrodes (cathode and anode) at constant pressure and with different amounts of Fe<sub>2</sub>O<sub>3</sub> nanoparticles. Calculations presented a reduction of the plasma emission intensity with the NPs content. Both the plasma density (calculated by Stark's broadening method) and the mean electron temperature (calculated using Boltzmann's equation) decreased with increasing the Fe<sub>2</sub>O<sub>3</sub> nanoparticles dust content, which indicates clearly the effect of dust density on restricting the movement of charge carriers, which in turn reduces inelastic plasma collisions.

**Keywords:** Dust plasma, mirror magnetron, electron temperature, electron density,

### تأثير غبار دقائق Fe<sub>2</sub>O<sub>3</sub> النانوية على خصائص بلازما التيار المستمر مع مغنطرون بشكل مرآة

شهد عماد الدين عبد الغني\*, قصي عدنان عباس

قسم الفيزياء, كلية العلوم, جامعة بغداد, بغداد, العراق

### الخلاصة

تم في هذا البحث دراسة تأثير غبار جسيمات اوكسيد الحديد النانوية (Fe<sub>2</sub>O<sub>3</sub> NPs) على معاملات بلازما التفريغ الكهربائي للتيار المستمر تحت الفراغ في الأرجون بوجود مغنطرون متقابل خلف كلا القطبين (الكاثود والانود) عند ضغط ثابت وبكميات مختلفة من الدقائق النانوية. أظهرت الحسابات أن شدة الانبعاث تتناقص مع زيادة محتوى المواد النانوية. وأظهرت حسابات كثافة الإلكترونات (المحسوبة بطريقة توسيع ستارك) ودرجة حرارة البلازما (باستخدام معادلة بولتزمان) نقصانها مع زيادة محتوى الدقائق النانوية والذي يدل على التأثير الواضح لكثافة الغبار على تقييد حركة حاملات الشحنة والذي بدوره يقلل من تصادمات البلازما غير المرنة.

\* Email: [shahademaduldeen@gmail.com](mailto:shahademaduldeen@gmail.com)

## 1. Introduction

In sputtering systems, the properties of deposition films can be significantly modified by controlling the flow of ions [1]. This process provides additional energies, which can modulate the nucleation process, and increase the deposition rate [2]. The energy and flux ions inside the plasma are intensely affected by the technique configuration. Generally, the plasma intensity is weak using the dc sputtering technique. So a skillful control is needed [3]. Magnetron sputtering technique has grown quickly in the last two decades, in response to the increased need for superior efficient films in many fields [4]. Magnetron sputtering now frequently outperforms alternative processes for coatings [1]. A magnetic field lines at specific design is exploited in magnetron sputtering to trap secondary electrons. This trapping effect raises plasma density between electrodes, causing the increase of the amount of ions hitting the target and, thus, obtaining faster deposition rates. Unbalanced magnetrons have a "leaky" magnetic field, which means that not all of the field lines between the center and outer poles are closed. Thin-film deposition can be controlled by changing the used magnetron design. By changing the composition of the magnetic field, the growth can be controlled with either low ion and/or electron attack, or by ions and/or electrons [5].

Dusty plasma, or complex plasma, contains micron-particles or nanoparticles suspended in it [6], which can be grown-up by the sputtered particles [7]. These large particles, compared with other plasma species, are hanging in plasma and charged with hundreds or thousands of electrons. So, due to the large surface charge of these large particles, they dominate the bulk plasma [8], they have a high influence on the plasma's behavior by changing charge distribution [9], and also cause magnetic distortion [10]. These plasmas have the additional difficulty of diagnosing the effect of this charged dust. Depending on the electrostatic coupling between the particles, the state of a dusty plasma changes from a weakly bound state to a liquid-like state and then to a crystalline state [11]. This plasma is of interest as a system for researching the general fundamental physics phenomena such as self-organization and phase transitions. [12]. Plasma with dust is investigated, in many types of research that have both physics studies and technological benefits. [16,17], to understand numerous phenomena as it is a component of the Earth's magnetosphere, cosmic plasma, and others [13-15]. Plasma diagnosis using emission spectroscopy is the famous, and most significant method to provide the plasma parameters [18].

The spread of dusty plasma concepts in many fields requires finding methods of diagnosing and controlling their parameters. In this study, the influence of Fe<sub>2</sub>O<sub>3</sub> NPs dust on plasma behavior and plasma parameters of dc discharge in argon under vacuum in mirror-magnetron configurations system at different NPs contents was investigated.

The Debye length in the plasma can be obtained as follows [19]:

$$\lambda_D = \sqrt{\frac{\epsilon_0 k_B T_e}{e^2 n_e}} \quad (1)$$

Where:  $\epsilon_0$  is the permittivity of free space,  $k_B$  is Boltzmann's constant,  $T_e$  is the electron temperature and  $e$  is the electron charge.

The plasma frequency is defined as [20]:

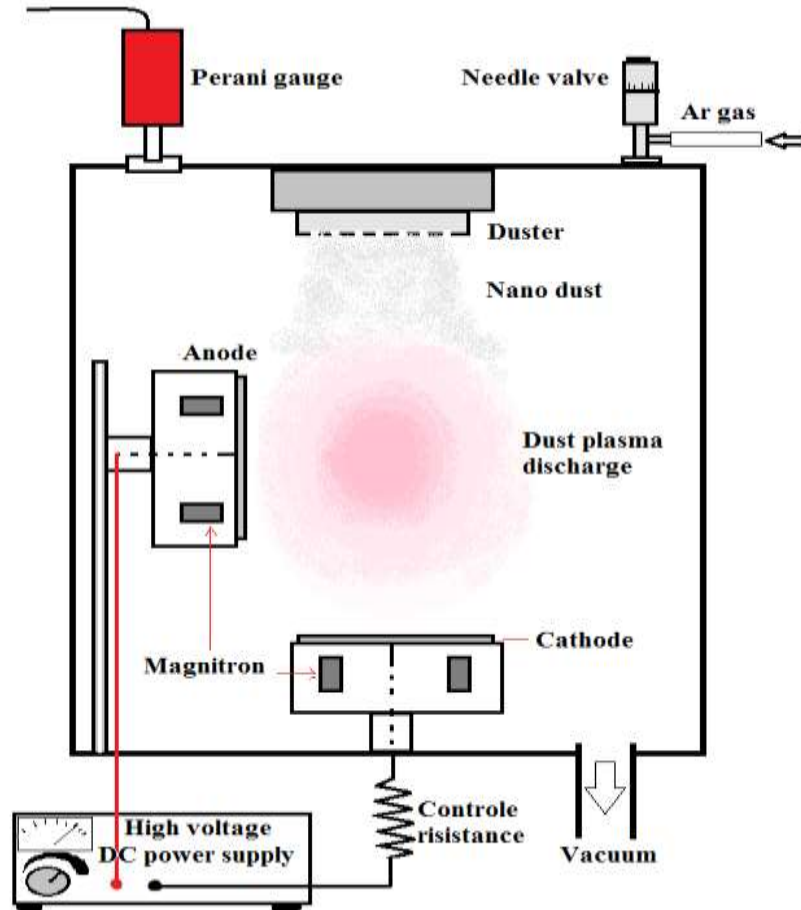
$$\omega_{pe} = \sqrt{\frac{n_e e^2}{m_e \epsilon_0}} \quad (2)$$

Where  $m_e$  is the electron mass.

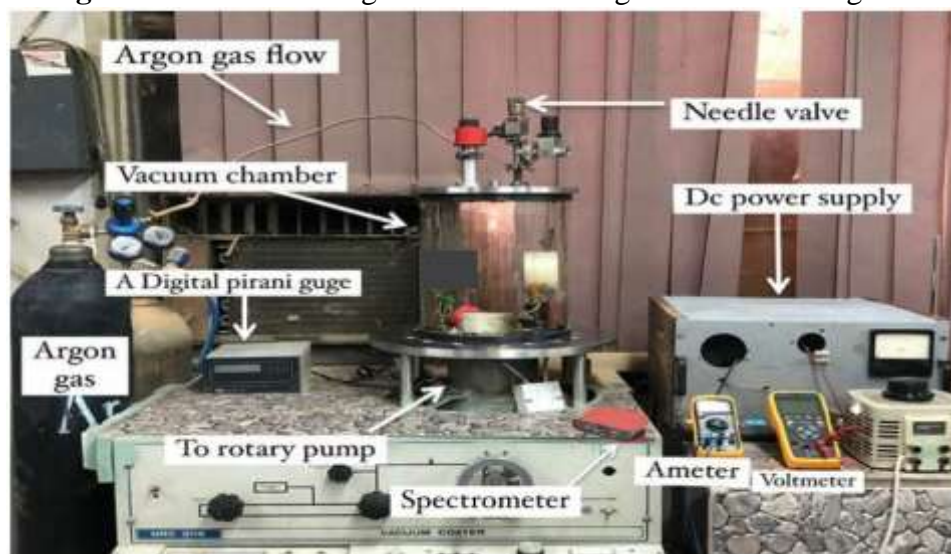
## 2. Experimental setup

The dc discharge configuration for this work is illustrated Figure 1 and Figure 2 shows the laboratory set-up. Two aluminum electrodes of 6 cm diameter were used. The two electrodes

were fixed perpendicularly to each other. A mirror magnetron of circular magnets was placed behind each electrode. The discharge was initiated with a DC high voltage of 3 kV in Ar under vacuum pressure of 0.4 Torr. Different amounts of  $\text{Fe}_3\text{O}_4$  NPs were dusted into the plasma from a duster attached to the chamber ceiling to investigate its effect on plasma behavior and parameters. Optical emission spectroscopy was employed to identify the plasma parameters at different dust contents.



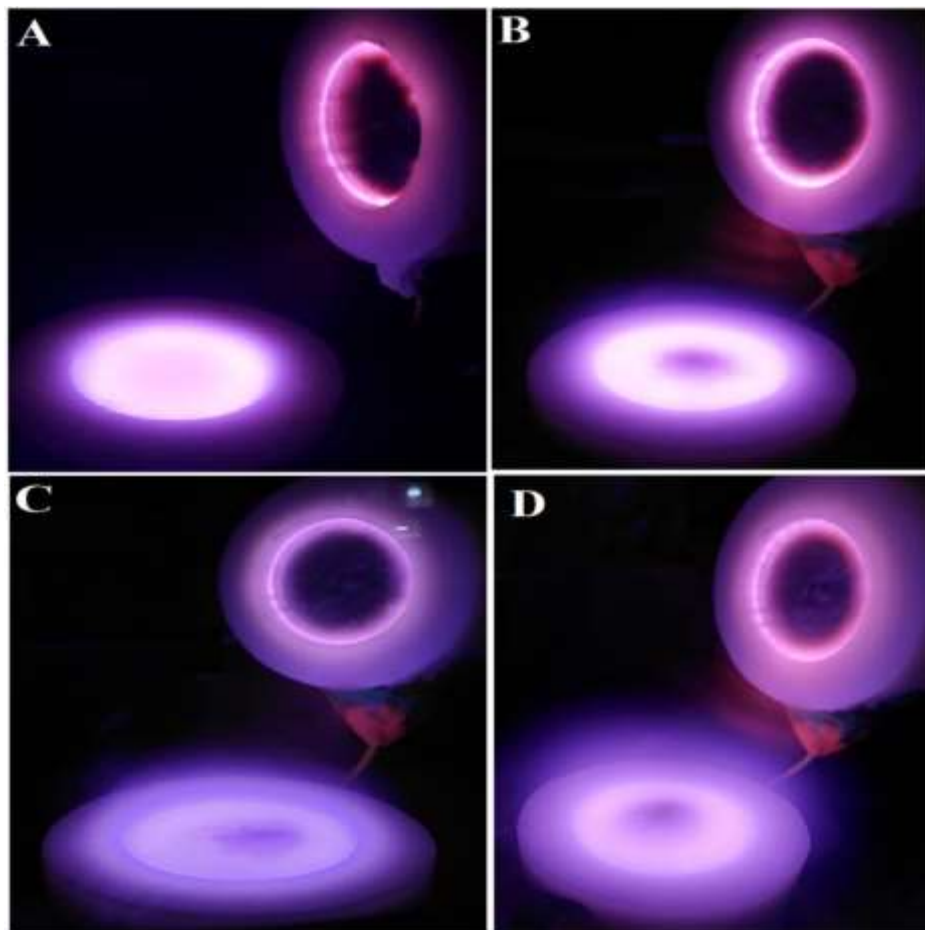
**Figure 1:** Schematic diagram of DC discharge with mirror magnetron.



**Figure 2:** DC discharge system of dust plasma set-up with mirror magnetron.

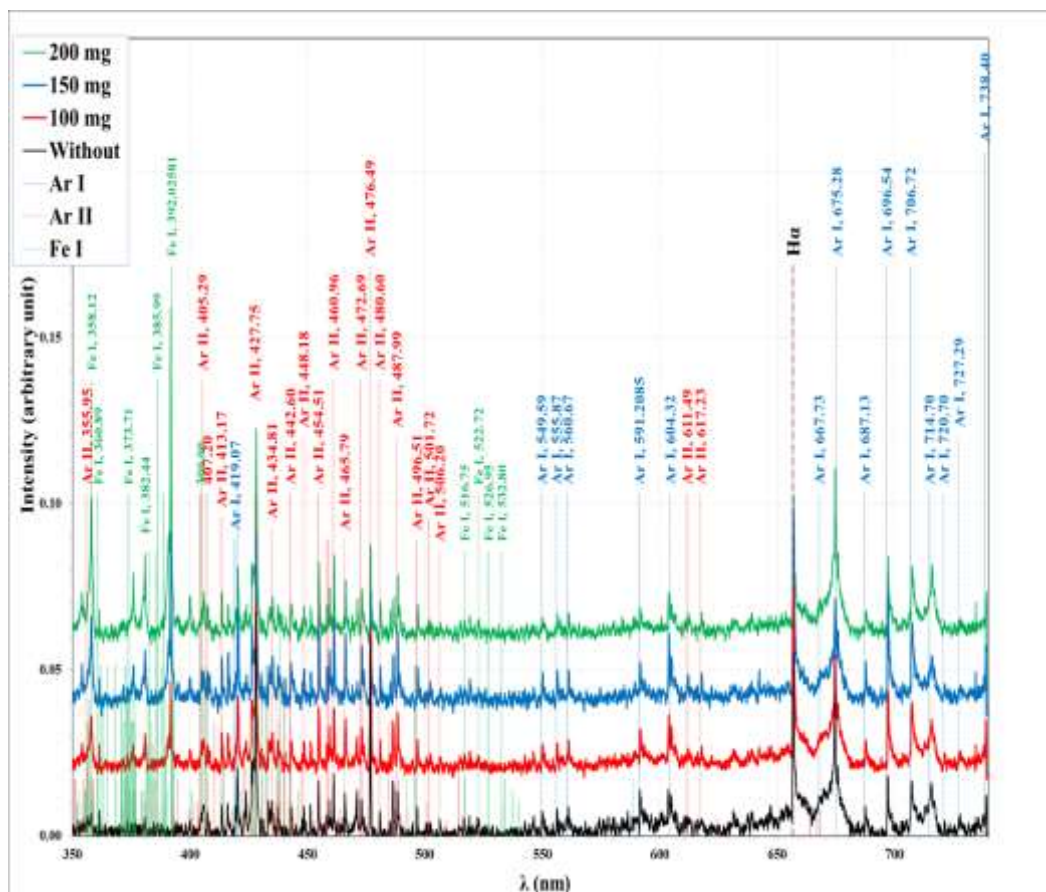
### 3. Results and Discussions

Figure 3 illustrates the plasma glow in argon gas of DC discharge with mirror configuration at 0.06 Torr pressure for the dust free and with different amounts of  $\text{Fe}_2\text{O}_3$  NPs (100, 150 and 200 mg). It clearly shows the suspended NPs within the plasma, which increases in clarity with increasing the  $\text{Fe}_2\text{O}_3$  NPs content. On the other hand, a decrease of plasma glow intensity was noticed with increasing the  $\text{Fe}_2\text{O}_3$  NPs content.



**Figure 3:** The effect of  $\text{Fe}_2\text{O}_3$  NPs on the plasma glow in DC discharge with mirror magnetron (A) without dust (B) with 100mg  $\text{Fe}_2\text{O}_3$ , (C) 150mg  $\text{Fe}_2\text{O}_3$  and (D) 200mg  $\text{Fe}_2\text{O}_3$ .

The emission spectra of dust-free plasma and dusted with different amounts of  $\text{Fe}_2\text{O}_3$  from dc discharge at 0.06 Torr argon pressure with mirror magnetron are exposed in Figure 4. Both atomic and ionic lines of argon appeared in the spectra indicating a partially ionized gas state. These lines vary in intensity according to the plasma temperature, the transition probability and the statistical weight of the upper levels, as described by the Boltzmann plot. A distinct line appeared at 656.7 nm corresponding to  $H\alpha$  line for residual hydrogen atoms after vacuum process. Additional peaks appeared corresponding to atomic iron lines. These lines increased in intensity, while the line intensity of argon decreased, with increasing the  $\text{Fe}_2\text{O}_3$  NPs contents.



**Figure 4:** DC discharge at 0.06 Torr argon pressure with mirror magnetron dusted with (a) 100mg Fe<sub>2</sub>O<sub>3</sub>, (b) 150mg Fe<sub>2</sub>O<sub>3</sub> and (c) 200mg Fe<sub>2</sub>O<sub>3</sub>.

The parameters of the selected argon lines used to measure the electron temperature ( $T_e$ ) are listed in Table 1, which shows wavelength,  $A_{ij}, g_j$ , upper and lower level energies ( $E_j, E_i$ ), and their level configurations from NIST site [21].

**Table 1:** Wavelength  $\lambda_{ij}$ ,  $A_{ij}, g_j$ , upper level energy  $E_j$ , and lower level energy  $E_i$  for ArI lines and their level configurations [21].

$\lambda$ (nm)	$g_k A_{ki}$	$E_i$ (eV)	$E_j$ (eV)	lower-level configuration	Upper-level configuration
555.8702	7.10E+06	12.90702	15.136848	$3s^2 3p^5 ({}^2P^\circ_{3/2}) 4p$	$3s^2 3p^5 ({}^2P^\circ_{3/2}) 5d$
560.6733	6.60E+06	12.90702	15.117746	$3s^2 3p^5 ({}^2P^\circ_{3/2}) 4p$	$3s^2 3p^5 ({}^2P^\circ_{3/2}) 5d$
603.212	2.21E+07	13.07572	15.130544	$3s^2 3p^5 ({}^2P^\circ_{3/2}) 4p$	$3s^2 3p^5 ({}^2P^\circ_{3/2}) 5d$
696.5431	1.90E+07	11.54835	13.327857	$3s^2 3p^5 ({}^2P^\circ_{3/2}) 4s$	$3s^2 3p^5 ({}^2P^\circ_{1/2}) 4p$
706.7218	1.90E+07	11.54835	13.302227	$3s^2 3p^5 ({}^2P^\circ_{3/2}) 4s$	$3s^2 3p^5 ({}^2P^\circ_{1/2}) 4p$
720.698	7.44E+06	13.30223	15.022088	$3s^2 3p^5 ({}^2P^\circ_{1/2}) 4p$	$3s^2 3p^5 ({}^2P^\circ_{1/2}) 6s$
727.2936	5.49E+06	11.62359	13.327857	$3s^2 3p^5 ({}^2P^\circ_{3/2}) 4s$	$3s^2 3p^5 ({}^2P^\circ_{1/2}) 4p$

Plasma temperature ( $T_e$ ) was calculated using Boltzmann plot for the discharge at different Fe<sub>2</sub>O<sub>3</sub> NPs contents (as revealed in Figure 5) according to the relation [22]:

$$\ln \left( \frac{I_{ji} \lambda_{ji}}{h c g_j A_{ji}} \right) = \left( -\frac{E_j}{k_B T_e} \right) + Constant \quad (3)$$

Where:  $I_{ji}$  is the intensity,  $A_{ji}$  is the probability of transition from  $i$  to  $j$ ,  $g_j$  is a statistical weight of upper  $j$  level,  $h$  is Planck's constant,  $\lambda_{ji}$  is the wavelength. The plasma temperature is equal to the inverse of the slope for the best linearly fit of the plot between  $\ln(I_{ij}\lambda_{ij}/hc g_j A_{ij})$  against the upper-level energies ( $E_j$ ).

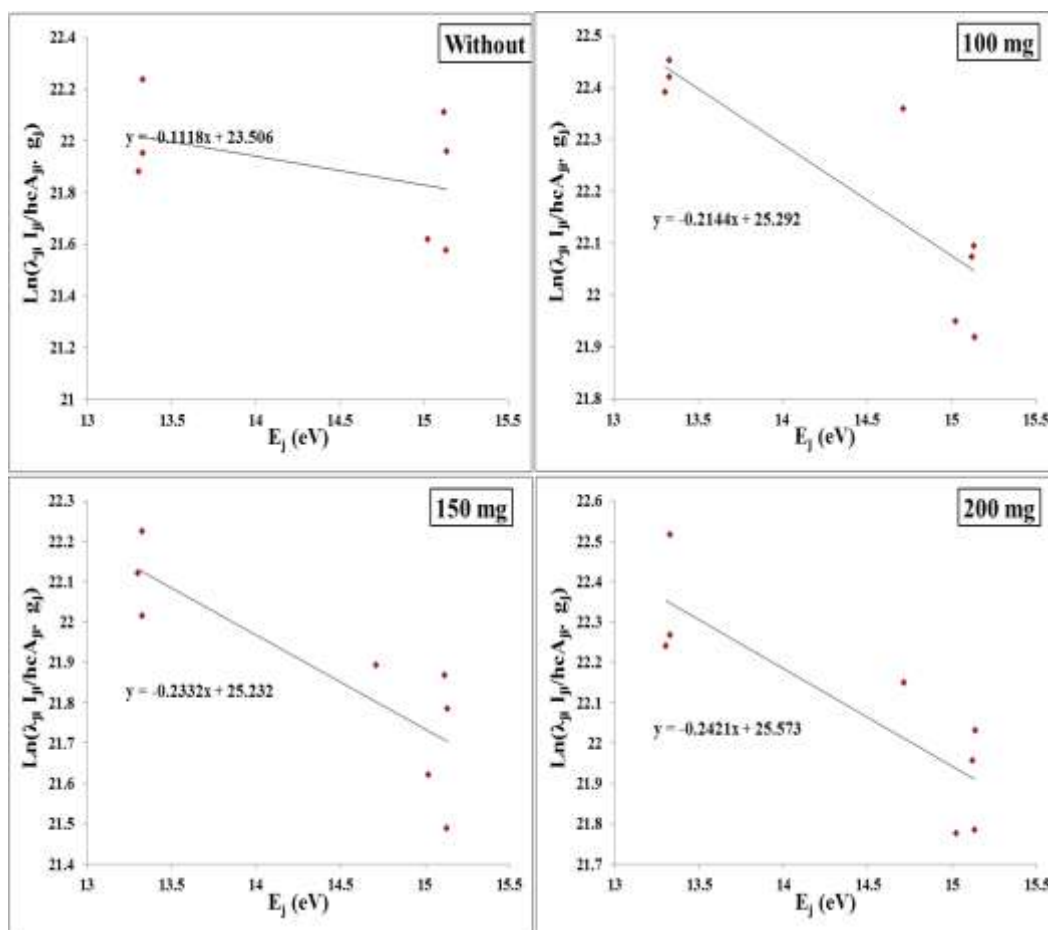


**Figure 5:** Boltzmann plots using eight of ArII lines for plasma at different Fe<sub>2</sub>O<sub>3</sub> NPs dust content.

The Stark broadening phenomena was used to calculate plasma density ( $n_e$ ) at different Fe<sub>2</sub>O<sub>3</sub> NPs contents using line broadening  $\Delta\lambda$  according to the following formula [23]:

$$n_e(cm^{-3}) = \left[ \frac{\Delta\lambda}{2\omega_s} \right] N_r \tag{4}$$

Where:  $\omega_s$  is the electron-impact value and  $N_r$  is the reference density.

The line broadening ( $\Delta\lambda$ ) For the ionic argon species at 476.49 nm for different Fe<sub>2</sub>O<sub>3</sub>NPs content were weighed by standard Lorentzian matching as illustrated in Figure 6. It appeared that the line width decreased slightly according to the Fe<sub>2</sub>O<sub>3</sub>NPs content indicating the reduction of the plasma density. Where the number of charges collected around the ion immersed into plasma is directly proportional to the density of the plasma. The decrease of plasma density leads to a reduction in the thickness of plasma shield thus reducing the applied electric field on the ion, which causes a change in the lines broadening of the plasma emission. The  $n_e$  was calculated using the Ar II 476.49 nm line parameters [24].

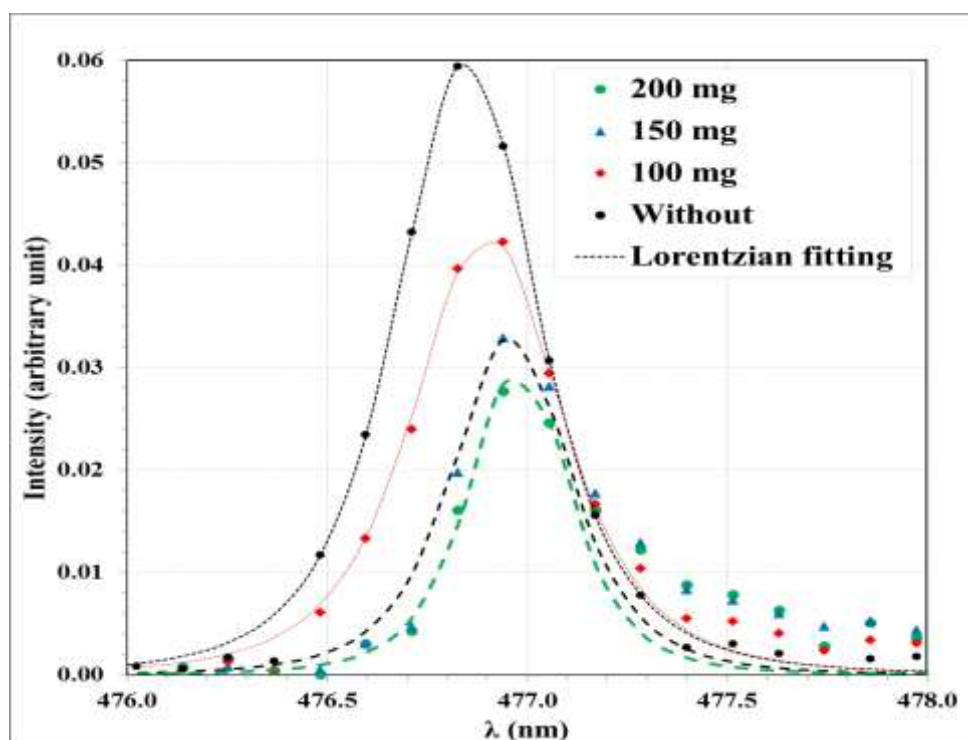


**Figure 6:** Lorentzian matching for the Ar II line at 476 nm for plasma at different NPs dust contents (dotted lines represent the standard Lorentzian curves).

Figure 7 displays the variation of plasma temperature and density with the  $\text{Fe}_2\text{O}_3$  NPs content. Both parameters decreased with the increase the  $\text{Fe}_2\text{O}_3$  NPs content from dust free up to 200 mg.  $n_e$  decreased from  $5.4 \times 10^{17}$  to  $3.9 \times 10^{17} \text{ cm}^{-3}$ , while  $T_e$  decreased from 8.94 to 4.13 eV. Increasing the dust content results in increased collisions with these particles causing the electrons to lose some energy which in turn reduces the possibility of ionizing collisions that perpetuate the density of the plasma, hence decreasing the plasma density [25].

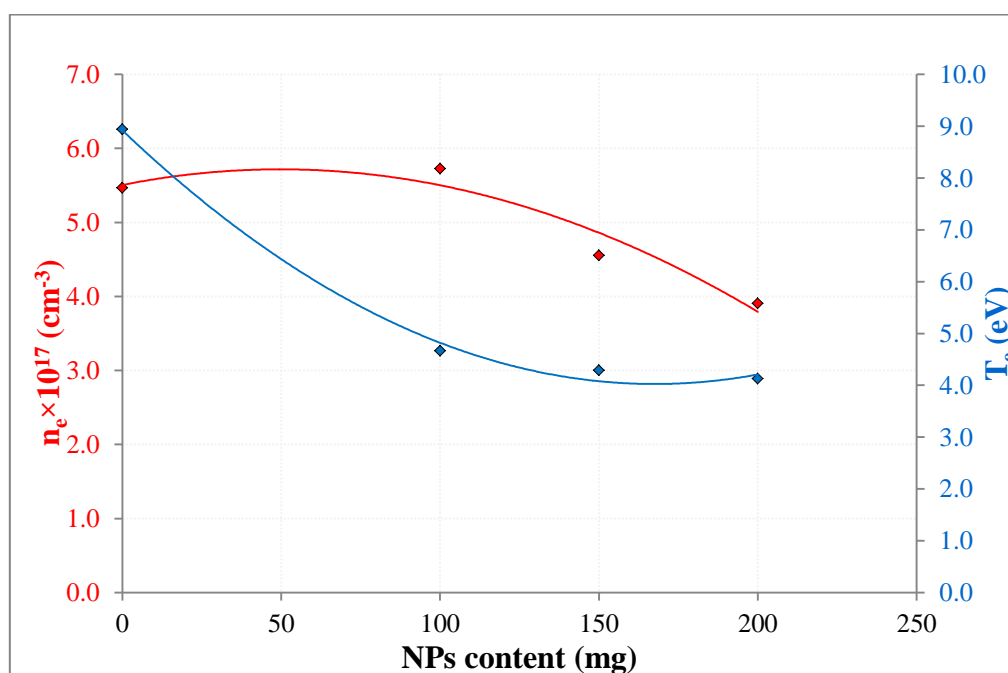


**Figure 7:** Variation of  $T_e$  and  $n_e$  with  $\text{Fe}_2\text{O}_3$  NPs dust contents for mirror magnetron dc discharge plasma.

Table 2 displays the parameters of dust plasma at different Fe<sub>2</sub>O<sub>3</sub>NPs contents. It is clear that the Debye length ( $\lambda_D$ ) (calculated from Eq. (1)) was reduced as a result of the reduction of plasma shielding effect with reducing density. The plasma frequency ( $f_p$ ) (calculated from Eq. (2)) was also reduced with increasing the dust content as it is directly related to the plasma density.

**Table 2:** Plasma parameters at different NPs dust Fe<sub>2</sub>O<sub>3</sub> contents for mirror magnetron dc discharge plasma.

Fe <sub>2</sub> O <sub>3</sub> (mg)	weight	T <sub>e</sub> (eV)	FWHM (nm)	n <sub>e</sub> × 10 <sup>17</sup> (cm <sup>-3</sup> )	f <sub>p</sub> × 10 <sup>12</sup> (Hz)	λ <sub>D</sub> × 10 <sup>-6</sup> (cm)	N <sub>d</sub>
0		8.945	0.420	5.469	6.641	3.005	62
100		4.664	0.440	5.729	6.797	2.120	23
150		4.288	0.350	4.557	6.062	2.279	23
200		4.131	0.300	3.906	5.613	2.416	23

#### 4. Conclusions

In this study, the effect of different contents of Fe<sub>2</sub>O<sub>3</sub> NPs dust on the DC discharge plasma across argon gas with mirror magnetron configuration was investigated. It was observed that the glow of plasma decreased with increasing the dust content due to the space charge carried by the dust particles that cause plasma complexity by distribution of electric field which cause to variation of plasma parameters. The plasma temperature and density were reduced with increasing the Fe<sub>2</sub>O<sub>3</sub> NPs content.

#### References

- [1] S. Kim, K.H. Kim, "Effect of Magnetic Field Arrangement of Facing Targets Sputtering (FTS) System on Controlling Plasma Confinement," *Coatings*, vol. 10, p. 321, 2020. <https://doi.org/10.3390/coatings10040321>
- [2] J. Lin, J.J. Moore, W.D. Sproul, B. Mishra, Z. Wu and J. Wang, "The structure and properties of chromium nitride coatings deposited using dc, pulsed dc and modulated pulse power magnetron sputtering," *Surf. Coatings Technol.*, vol. 204, no. 14, pp. 2230–2239, 2010. <https://doi.org/10.1016/j.surfcoat.2009.12.013>
- [3] G. Shanker, P. Prathap, K.M.K. Srivatsa and P. Singh, "Effect of balanced and unbalanced magnetron sputtering processes on the properties of SnO<sub>2</sub> thin films," *Curr. Appl. Phys.*, vol. 19, no. 6, pp. 697–703, 2019. <https://doi.org/10.1016/j.cap.2019.03.016>
- [4] J.R. Gaines, "The Effect of Sputter Cathode Design on Deposition Parameters," *Vak. Forsch. Und Prax.*, vol. 31, no. 5, pp. 14–19, 2019. <https://doi.org/10.1002/vipr.201900718>
- [5] B. Tian, Q. Yu, Z. Zhang, Z. Du, W. Ren, P. Shi and Z. Jiang, "Effect of magnetron sputtering parameters on adhesion properties of tungsten-rhenium thin film thermocouples," *Ceram. Int.*, vol. 44, Supplement 1, pp. S15–S18, 2018. <https://doi.org/10.1016/j.ceramint.2018.08.334>
- [6] E.S. Dzljeva, V.Y. Karasev and S.I. Pavlov, "Dynamics of Plasma–Dust Structures Formed in a Trap Created in the Narrowing of a Current Channel in a Magnetic Field," *Dusty Plasma*, vol. 42 pp.142–149, 2016. <https://doi.org/10.1134/S1063780X16020033>
- [7] V. Vekselman, Y. Raitses and M.N. Shneider, "Growth of nanoparticles in dynamic plasma," *Phys. Rev. E.*, vol. 99, no. 6, 063205, 2019. <https://doi.org/10.1103/PhysRevE.99.063205>
- [8] T.F. Toussaint, "The charge distribution of dust particles in plasma afterglow, *Faculteit Technische Natuurkunde*," 2017.
- [9] L.G. D'yachkov, O.F. Petrov and V.E. Fortov, "Dusty Plasma Structures in Magnetic DC Discharges," *Contrib. Plasma Phys.*, vol. 49, no. 3, pp. 134 – 147, 2009. <https://doi.org/10.1002/ctpp.200910017>
- [10] M.W. Morooka, J.E. Wahlund, D.J. Andrews, A.M. Persoon, S.Y. Ye, W.S. Kurth, D.A. Gurnett and W.M. Farrell, "The Dusty Plasma Disk Around the Janus/Epimetheus Ring," *J. Geophys.*

- Res. Sp. Phys.*, vol. 123, no. 6, pp. 4668–4678, 2018. <https://doi.org/10.1002/2017JA024917>
- [11] E.S. Dзлиeva, L.G. D'yachkov, L.A. Novikov, S.I. Pavlov and V.Y. Karasev, "Dusty Plasma in Inhomogeneous Magnetic Fields in a Stratified Glow Discharge," *Molecules*, vol. 26, no. 13, 3788, 2021. doi: [10.3390/molecules26133788](https://doi.org/10.3390/molecules26133788)
- [12] G.E. Morfill and A. V. Ivlev, "Complex plasmas: An interdisciplinary research field," *Rev. Mod. Phys.*, vol. 81, no. 4, pp.1353–1404, 2009. <https://doi.org/10.1103/RevModPhys.81.1353>
- [13] N. Borisov and H. Krüger, "Formation of the The be Extension in the Ring System of Jupiter," *J. Geophys. Res. Sp. Phys.* vol. 126, no. 11, pp.1–13, 2021. <https://doi.org/10.1029/2021JA029654>
- [14] N. Borisov and H. Krüger, "Formation of the The be Extension in the Ring System of Jupiter," *J. Geophys. Res. Sp. Phys.* vol. 126, no. 11, pp.1–13, 2021. <https://doi.org/10.1029/2021JA029654>
- [15] J.G. Choi, H.Y. Kim and H.B. Lim, "Analysis of ferrite powder using inductively coupled plasma atomic emission spectrometry," *Microchem. J.*, vol. 63, no. 1, pp.119–127, 1999. <https://doi.org/10.1006/mchj.1999.1773>.
- [16] B. Lindstrom, P. Bélanger, A. Gorzawski, J. Kral, A. Lechner, B. Salvachua, R. Schmidt, A. Siemko, M. Vaananen, D. Valuch, C. Wiesner, D. Wollmann and C. Zamantzas, "Dynamics of the interaction of dust particles with the LHC beam," *Phys. Rev. Accel. Beams.*, vol. 23, no. 12, 124501, 2020. <https://doi.org/10.1103/PhysRevAccelBeams.23.124501>
- [17] R. Merlino, "Dusty plasmas: from Saturn's rings to semiconductor processing devices," *Adv. Phys. X.*, vol. 6, no. 1, 2021. <https://doi.org/10.1080/23746149.2021.1873859>
- [18] M. Zhukov, "Plasma Diagnostics," Lightning Source UK Ltd, Mosco, 2005.
- [19] Ali A-K. Hussain, Kadhim A. Aadim and Waleed I. Yaseen, "Diagnostics of low-pressure capacitively coupled RF discharge argon plasma," *Iraqi Journal of Physics*, vol.13, no.27, pp.76-82, 2019.
- [20] Marieam G. Jasim and Qusay A. Abbas, "Influence of working pressure and lasing energy of Al plasma in laser-induced breakdown spectroscopy," *Iraqi Journal of Physics*, vol.17, no.40, pp.59-66, 2019.
- [21] NIST Atomic Spectra Database, (n.d.).
- [22] S.S. Hamed, "Spectroscopic Determination of Excitation Premixed Laminar Flame," *Egypt. J. Solids*. vol. 28, no. 2, pp. 349–357, 2005.
- [23] N.M. Shaikh, S. Hafeez, B. Rashid and M.A. Baig, "Spectroscopic studies of laser induced aluminum plasma using fundamental, second and third harmonics of a Nd: YAG laser," *Eur. Phys. J. Journal D.*, vol.44, pp. 371–379, 2007. <https://doi.org/10.1140/epjd/e2007-00188-3>
- [24] N. Konjević and W.L. Wiese, "Experimental Stark widths and shifts for spectral lines of neutral and ionized atoms," *J. Phys. Chem. Ref. Data.*, vol. 19, no. 6, pp.1307–1385, 1990. <https://doi.org/10.1063/1.555847>
- [25] A. Ahmed, M.O. Salman, M. Alwazzan and A. Meri, "Blushers Component Analysis for Unbranded Cosmetic Brands: Elements Concentration Levels and its Effect on Human Body," *Jour Adv Res. Dyn. Control Syst.* 2, pp.1–8, 2019.